JOURNAL OF APPLIED ELECTROCHEMISTRY 7 (1977) 473–484

Enhanced mass transfer in electrochemical cells using turbulence promoters

F. B. LEITZ*, L. MARINČIĆ†

Ionics, Inc., Watertown, Massachusetts, USA

Received 22 February 1977

Many electrochemical processes suffer in varying degrees from mass transfer limitations. These limitations may require operation at considerably less than economic optimum current densities. Mass transfer to a surface may be considerably enhanced by insertion of turbulence promoters in the fluid flow path near the affected surface.

An instrument was developed to measure local current densities in the hydrodynamically very difficult region near the turbulence promoter. A general method for the relative evaluation of hydrodynamic conditions has been developed. Generalization of the data permits optimization of hydrodynamic cell design using the promoter shapes investigated.

Notation

Symbols

A	Coefficient for cell power costs, $\$\,m^2\,(A\,s)^{-1}$
A_c	Cell area, m^2
a	Constant in Equation 4
B	Coefficient for area-proportional costs, $\$\,A\,(m^2\,s)^{-1}$
C	Coefficient for pumping power costs, $\$\,A\,(m^2\,s)^{-1}$
C_b	Bulk concentration, $kg\,mol\,m^{-3}$
C_{bi}	Inlet bulk concentration, $kg\,mol\,m^{-3}$
C_e	Energy cost, $\$\,(W\,s)^{-1}$
C_i	Interfacial concentration, $kg\,mol\,m^{-3}$
$\bar{C}_s$	Amortized area cost, $\$\,(m^2\,s)^{-1}$
D	Current–density-insensitive costs, $\$\,s^{-1}$
D_e	Equivalent diameter, m
$\mathfrak{D}$	Diffusion constant, $m^2\,s^{-1}$
e	Current efficiency
F_d	Cell feed rate, $m^3\,s^{-1}$
$\mathcal{F}$	$96{\cdot}5 \times 10^6\,A\,s\,kg\,eq^{-1}$
g	Channel width, m
h	Channel height, m
i	Current density, $A\,m^{-2}$
i_{opt}	Economic optimum current density, $A\,m^{-2}$
K	Total costs of running cell, $\$\,s^{-1}$
$(K-D)_{ideal}$	Total sensitive costs under hydrodynamically ideal conditions, $\$\,s^{-1}$
k_c	Convective mass transfer coefficient, $m\,s^{-1}$
L	Total length of flow path, m
Δl	Promoter spacing, m
N	Mass flow rate to surface due to convection, $kg\,mol\,m^2\,s^{-1}$
n_e	Number of electrons transferred in electrode reaction
P_c	Power required by cell, W
$\Delta P/L$	Average pressure gradient in channel, $N\,m^{-3}$
R_{av}	Effective cell resistance, $\Omega\,m^2$
S	Open channel cross-section, m^2
S_0	Minimum channel cross-section at promoter, m^2
s_i	Stoichiometric coefficient of species i
t_i	Transport number of species i in solution
$\bar{t}_i$	Effective tranport number of species at polarized surface
V	Average fluid velocity, $m\,s^{-1}$

Present addresses: * Bureau of Reclamation, Denver, Colarado and † E. P. Joslin Research Laboratory, Harvard Medical School, Boston, Massachusetts.

x	Distance from inception of concentration disturbance, m
η_1	Electrical power conversion efficiency
η_2	Pumping power conversion efficiency
μ	Solution viscosity, $kg\,(m\,s)^{-1}$
ρ	Solution density, $kg\,m^{-3}$

Dimensionless groups

$f \equiv \frac{\Delta P}{L}\frac{D_e}{2\rho V^2}$	Fanning friction factor
$(Re) \equiv \frac{D_e V \rho}{\mu}$	Reynolds number
$R \equiv h/g$	Channel aspect ratio
$\frac{D_e}{\Delta l}$	Promoter frequency
$\beta \equiv \frac{S}{S_0}$	Contraction coefficient
$(Sh) \equiv \frac{k_c D_e}{\mathfrak{D}}$	Sherwood number
$f_0 \equiv \frac{C_{bi} - C_0}{C_{bi}}$	Degree of reaction
$\frac{K-D}{(K-D)_{ideal}}$	Dimensionless total sensitive costs
$i\left(\frac{C_e R_{av}}{\bar{C}_s \eta_1}\right)^{1/2}$	Dimensionless current density
$N_{ec} \equiv \frac{C_e \mu^3}{\bar{C}_2 \rho^2 D_e^3 \eta_2}$	Energy cost ratio

1. Introduction

The optimization of electrochemical systems generally requires high rates of energy input. Frequently, this means that high rates of mass transfer are required to a surface from the bulk of a flowing stream. A common practice is to place hydrodynamic obstructions or 'turbulence promoters' in the flowing stream to break up the mass transfer boundary layer. The purpose of this investigation was to measure the local values of mass transfer produced by certain types of turbulence promoters, to select the best of existing promoters and to determine their overall economic effect.

The cell consists of a chamber of rectangular cross-section, the two long sides of which consist of plane parallel electrodes or a plane parallel electrode and membrane or hydraulically impermeable separator. This is sketched in Fig. 1. The electrode reaction follows the general scheme

$$s_1X_1 + s_2X_2 \rightarrow s_3X_3 + s_4X_4 + n_e e^- . \quad (1)$$

The reaction proceeds in the liquid phase and is limited by mass transfer of species i to one of the plane surfaces subsequently called the polarized surface. Mass transfer is negligibly affected either by density differences or by evolution of gas in the cell.

Insertion of turbulence promoters into a flowing stream increases the pressure drop through the apparatus, thus increasing the requirement for pumping energy. It is necessary to measure both the mass transfer rate obtainable with a promoter and the pressure drop resulting from it at a given fluid velocity. Cost optimization requires a minimization of the sum of capital cost amortization, process energy cost and pumping energy cost.

A unique aspect of the present study was the quantitative measurement of local mass transfer profiles around each turbulence promoter. The results of this study are potentially applicable to a wide variety of chemical cell design problems.

2. Segmented electrode apparatus

An apparatus was developed to measure maximum local rates of mass transfer in rectangular channels near a turbulence promoter. The instrument consisted of an electrochemical cell assembly and a data acquisition system. The flow system consisted of a solution reservoir, pump, surge tank, filter, test cell and rotameter and is sketched in Fig. 2. Solution temperature in the reservoir was maintained at 298 K.

In order to measure the local current density, a portion of the cathode is segmented (sketched in Fig. 1). The segmented portion consists of an array of 50 rows each containing 20 segments which are circular in cross-section (with a diameter of $2{\cdot}5 \times 10^{-4}$ m) and close-packed on triangular centres. Measurement of the current passing through each segment of the cathode provides a comprehensive profile of the effect of a turbulence promoter on mass transport.

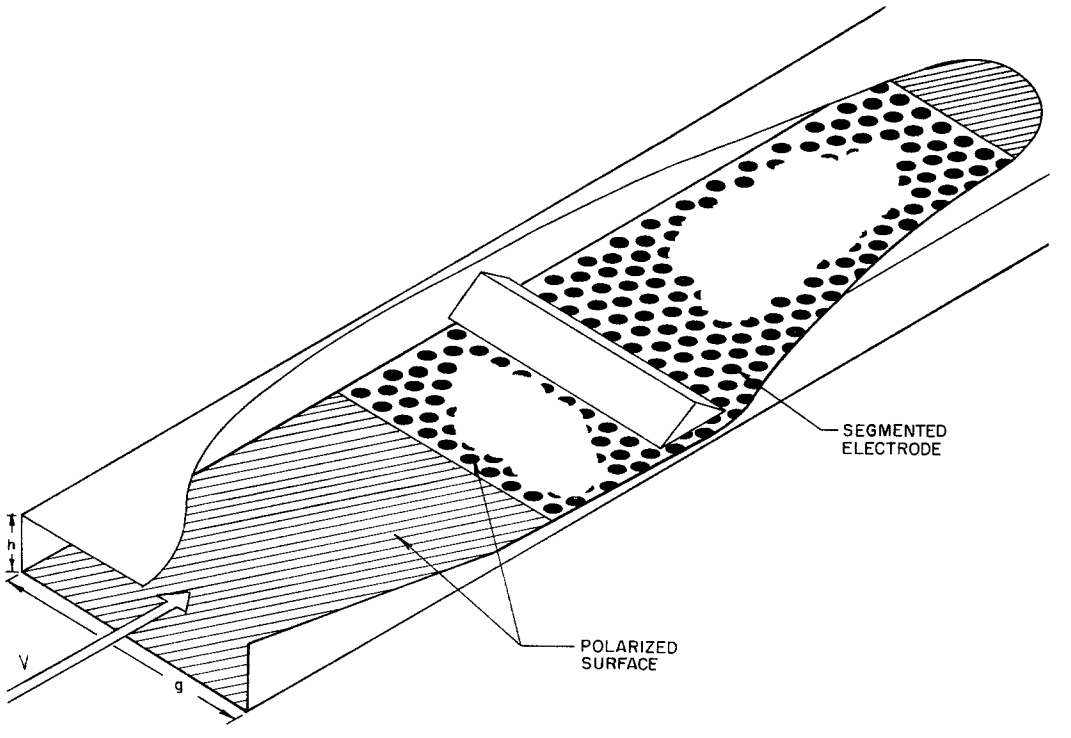

Fig. 1. Sketch of test cell with promoter.

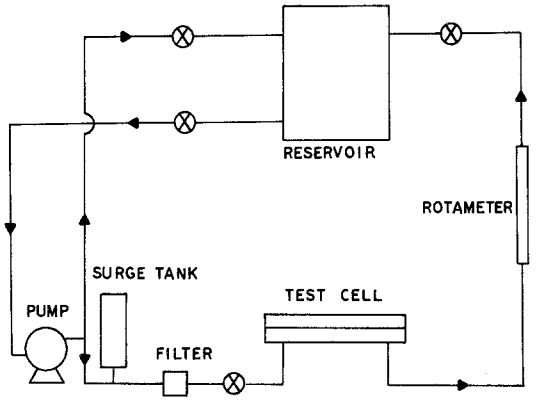

Fig. 2. Electrochemical cell assembly.

The electrochemical cell is of plate and frame construction. It contains stainless steel end plates and through bolts, lucite end blocks, an anode and cathode of platinum plated titanium (except for the segmented portion of the cathode, which was made of platinum) and spacers cut from sheets of polyethylene. The spacers and electrodes confine a channel of rectangular cross-section whose dimensions can be changed by insertion of an appropriate spacer. The rectangular and triangular turbulence promoters were integral with one of the spacer sheets; the circular promoters were inserted between or under the sheets.

Typical dimensions of the channel parameters as designated in Fig. 1 were $h = 1{\cdot}02 \times 10^{-3}$ m, $g = 6{\cdot}35 \times 10^{-3}$ m, and promoter dimensions, thickness $(h/2) = 5{\cdot}1 \times 10^{-4}$ m and base of the triangle $= 2{\cdot}5 \times 10^{-3}$ m. Fluid velocity varied between 0·25 and 1·00 m s^{-1}.

A differential manometer measured the pressure drop over a fixed length of channel. In order to prevent possible disruption of the flow patterns and distortion of the mass transfer profile by the upstream manometer, the pressure drop was measured in separate runs using a special top plate which had provisions for the attachment of the manometer.

Potassium ferricyanide/ferrocyanide in basic solution was found to give reproducible polarization curves in which the current was proportional to the concentration of the reducible ion and almost independent of applied voltage over a range of 500 mV. Potassium hydroxide, 0·1 N, was used as supporting electrolyte. This work is described in detail in [1].

In its simplest form, the segmented electrode can be considered as a portion of a coil of insulated wire, a part of which has been potted in epoxy and cut across both in the potted and in the unpotted parts. The potted part provides the active electrode surface while the unpotted part permits connections to the separate segments to be made.

The data acquisition system consists of a transducer in the circuit of each electrode segment, a 1000-channel data logger which converts the output of these transducers, in sequence, to a digital signal and a paper tape punch for recording the digital information. The transducers are 10 kΩ precision resistors which produce a voltage proportional to the current passing through the electrode segments.

A period of 17 min is required for a complete data scan. In order to avoid the bias which could result if the segment were measured in order, say from front to back of the electrode, the readings were taken in a randomized fashion. Each column of 50 was divided into 5 groups of 10 electrodes. The group of 10 were measured in randomized sequence.

In order to test the unit, data were taken under hydrodynamic conditions where a theoretical expression for mass transfer exists. Runs were made in laminar flow with no current flowing through the plate cathode, i.e. with the concentration disturbance beginning at the leading edge of the segmented electrode.

For laminar flow between parallel plates of infinite width with an already well-established velocity profile and negligible ion migration, Newman [2] presents the expression:

$$i = 0{\cdot}9783 \frac{n_e \mathcal{F} \mathcal{D} C_b}{s_i} \left(\frac{V}{h \mathcal{D} x} \right)^{1/3}. \qquad (2)$$

In order to compensate for the area of the segmented electrode which is not electrochemically active, the total area subtended by the electrode divided by 1000 was used for the effective area of each segment. This assumes that the electrode is sufficiently fine-grained that the concentration profile is not disturbed greatly. Good agreement was obtained between such data and Equation 2.

3. Pressure drop in rectangular channels

The pressure drop per unit length in a rectangular channel is given by:

$$\frac{\Delta P}{L} = \frac{V\mu}{h^2/12 - \sum_{n\text{-odd}} 16h^3/[(n\pi)^5 g] \tanh n\pi g/2h}. \qquad (3)$$

Equation 3 can be expressed dimensionlessly as:

$$f = a/(Re). \qquad (4)$$

For a characteristic length the equivalent diameter was used and defined by:

$$D_e \equiv \frac{2gh}{g+h}. \qquad (5)$$

With this definition, the constant a is a function of the ratio of linear dimensions varying from 14·2 for a channel of square cross-section ($h/g = 1$) to 24·0 for infinite parallel plates ($h/g = 0$). For channels having a width at least twice the height, an approximation within 0·5% is:

$$a = 1/0{\cdot}0417 + 0{\cdot}0572R - 0{\cdot}0106R^2 - 0{\cdot}0261R^3 \qquad (6)$$

where

$$R \equiv h/g. \qquad (7)$$

Measurements of pressure drop were made in channels of 0·05 to 0·1 cm nominal height. Promoters which were circular, rectangular and triangular in cross-section were tested. With the circular promoters in the test section, the ratio of diameter to channel height and the position in the channel were varied. With rectangular promoters the length of the promoter in the flow direction was varied. With triangular promoters, the position of the promoter in the channel was varied. These data are presented in [3].

The pressure drop is a function of Reynolds number, promoter frequency and the ratio of promoter height to channel height. For all circular and triangular promoters, the data can be well correlated by:

$$f = \frac{a}{(Re)} + 0{\cdot}175 \frac{D_e}{\Delta l} \frac{1-\beta^2}{\beta^2}. \qquad (8)$$

Most values are within 10% of the prediction and only a rare value is more than 15% in error. Data for rectangular promoters are correlated by:

$$f = \frac{a}{(Re)} + 2{\cdot}082 \frac{D_e}{\Delta l}. \qquad (9)$$

The pressure drop was not significantly affected by the length of the promoter in the direction of flow.

These functions express the pressure drop as a sum of a laminar term and a turbulent term. The laminar term is equal to that measured for the open channel without promoters. The turbulent term describes the eddying which results from insertion of the promoters.

There are velocity limitations to these correlations. At sufficiently low linear velocities, the momentum of the flowing stream is insufficient for the promoter to cause turbulence so that creeping flow occurs. At sufficiently high linear velocities, a stage is reached where laminar flow becomes unstable. Since there are turbulence promoters present, the transition out of laminar flow occurs at lower Reynolds numbers than in chanels without promoters. With circular and rectangular promoters the lower transition occurs at a Reynolds number of about 250 and the upper transition at about 1850. With triangular promoters the range of linearity appears to be wider, the lower transition occurring at about 200 and the upper transition at about 2000.

4. Mass transfer in rectangular channels

The effect of rectangular, triangular and circular promoters on mass transfer to the channel wall was studied extensively. Four locations were employed. 'Attached', 'opposed' and 'detached' refer respectively to the location of the promoter against the polarized surface, against the non-polarized surface and centered in the channel. In the detached position the peak of the triangular promoter was as far from one surface as the base was from the other. The detached triangular promoter was studied in two positions: in the A position, with the point of the triangle toward the non-polarized surface, and in the V position, with the point toward the polarized surface.

Data from runs with various promoters were reduced to mass transfer profiles. Profiles for opposed rectangular promoters are shown in Fig. 3. The balance of the profiles appear in [3]. The plotted printouts of most of the data from which these profiles were made are found in [4].

The method of calculating average current density for a particular promoter type position size and frequency was to integrate under the mass transfer profile for a distance of one promoter interspace and divide by the promoter spacing. All mass transfer profiles measured have one consistent characteristic: following the last peak in current density there is a slow decrease in current density with increasing distance from the promoter. In this region the flow perturbations and the concentration irregularities are slowly relaxing. The current densities measured in this region can be closely fitted by an exponential function.

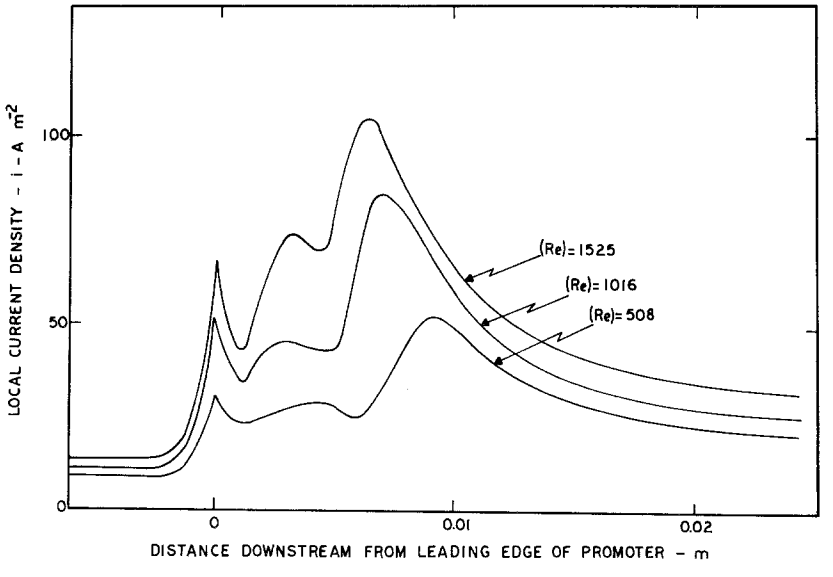

Fig. 3. Mass transfer profiles with opposed rectangular promoter.

A general correlation for each promoter position was obtained by expressing the current density as a power function of (Re) and $D_e/\Delta l$. The coefficients were determined by multiple least squares regression after which values were calculated from the derived expressions for comparison to the data values. Generally, the correlations are very good; few calculated values being more than 10% away from the data values. The worst fit uniformly occurs at the highest values of $D_e/\Delta l$ where the relatively low current densities upstream of the current peak begin to be a large portion of the total. It was obvious in some cases that the current densities at high values of $D_e/\Delta l$ would not fit this form of correlation well. In these cases such values were not used to establish the coefficients in the equations.

These results were generalized by the use of the appropriate dimensionless groups. This requires the introduction of the Sherwood number and the Schmidt number.

A local one-dimensional convection mass transfer coefficient is defined by the equation:

$$N = k_c(C_b - C_i). \tag{10}$$

This coefficient can be related to the current density where both convection and electrical transport are operative by:

$$i = \frac{k_c n_e (C_b - C_i)\mathcal{F}}{s_i(\bar{t}_i - t_i)}. \tag{11}$$

Where the affected surface is a membrane or porous separator, $\bar{t}_i$ is the transport number of species i in the membrane or separator. If the affected surface is an electrode, $\bar{t}_i$ is the current efficiency defined as the fraction of the current involved in the reaction concerning species i.

The Sherwood number can then be expressed as:

$$(Sh) \equiv \frac{k_c D_e}{\mathcal{D}} = \frac{i(\bar{t}_i - t_i)D_e s_i}{n_e \mathcal{F}(C_b - C_i)\mathcal{D}} = \frac{i_{lim}(\bar{t}_i - t_i)D_e s_i}{n_e \mathcal{F} C_b \mathcal{D}}. \tag{12}$$

In much of the literature on electrochemical mass transfer, the experiments are run, as they were in this study, with a large excess of supporting electrolyte so that $\bar{t}_i - t_i \cong 1{\cdot}0$. However, in many electrochemical applications this is not the case.

The power on the Schmidt number has been assumed to be 1/3. The generalized correlations are given in Table 1.

5. Optimization of cell hydrodynamics

To observe the effect of variables on the economics of cell operation, the total cost per unit operation should be determined. An equation of total cost per unit time can be obtained by summing costs of cell power, area proportional costs, pumping power costs and current density insensitive costs. Expressing these as functions of current density:

$$K = Ai + B/i + C/i + D. \tag{13}$$

It is convenient to express costs in terms of current density since the expressions for electrochemical reaction relate conceptually most directly to current or current density. However, there may be optimum current density only for a differential degree of reaction. For a cell of finite electrode length, the current density will generally vary along the flow path. By contrast, the applied voltage is essentially constant. When we speak of optimum current density below, we refer to the average current density which corresponds to the optimum applied voltage for the cell under consideration.

The cost factors in Equation 13 can be identified for a stage fed at a rate F_d with a concentration C_{bi} and run to yield a degree of reaction f_0 as follows:

$$Ai = \frac{C_e P_c}{\eta_1} = \frac{C_e F_d C_{bi} f_0 \mathcal{F} n_e R_{av} i}{\eta_1 e s_i} \tag{14}$$

$$\frac{B}{i} = \bar{C}_s A_c = \frac{\bar{C}_s F_d C_{di} f_0 \mathcal{F} n_e}{e i s_i} \tag{15}$$

$$\frac{C}{i} = \frac{C_e(\Delta P/L)VhA_c}{\eta_2} = \frac{C_e(\Delta P/L)VhF_d C_{bi} f_0 \mathcal{F} n_e}{\eta_2 e i s_i}. \tag{16}$$

Some components of these equations require comments. In Equation 14, η_1 is the efficiency of power conversion. This equation contains no explicit provision for amortization of the rectifier, which generally amounts to a few percent of the cost of power unless the rectifier is being amortized very rapidly. To include this factor, rectifier amortization can be expressed by decreasing η_1 appropriately.

The effective cell resistance, R_{av}, is the slope of the best straight line that can be drawn through a plot of cell voltage versus current density.

Over a wide range of capacities, cell capital cost

can be expressed as a unique function of active all pair area. This cost is not directly proportional to active area but, for modest ranges, can be accurately expressed as a linear function of active area with a positive intercept. The intercept value should be added to the insensitive costs.

The term D is not easily generalized. It includes part of the installed capital cost and part of the total power cost. While there is some relationship between the number of cells and the labour force required, it appears most satisfactory to include labour cost in D. The term D is carried through this formalization as a reminder that such costs are not negligible.

Moving the term D to the left-hand side of Equation 13, the total sensitive costs can be written:

$$K - D = Ai + B/i + C/i. \tag{17}$$

The optimum (average) current density is:

$$i_{\text{opt}} = \left(\frac{B + C}{A}\right)^{1/2}. \tag{18}$$

Normalizing the current density in Equation 17 with i_{opt}:

$$K - D = A^{1/2}(B + C)^{1/2}\left(\frac{i}{i_{\text{opt}}} + \frac{i_{\text{opt}}}{i}\right). \tag{19}$$

Under hydrodynamically ideal conditions $i = i_{\text{opt}}$ and C is negligible compared to B.
Hence,

$$(K - D)_{\text{ideal}} = 2A^{1/2}B^{1/2}. \tag{20}$$

The total cost can be normalized with respect to this ideal cost:

$$\frac{K - D}{(K - D)_{\text{ideal}}} = \left(1 + \frac{C}{B}\right)^{1/2}\left(\frac{i/i_{\text{opt}} + i_{\text{opt}}/i}{2}\right). \tag{21}$$

Equation 21 is particularly interesting in that it expresses the normalized sensitive costs as the product of two terms each of which is at least equal to but is generally greater than unity. The first term expresses the effect of the costs of pumping the solution. The second term shows the result of operating below optimum current density. Both of these terms are sensitive to the Reynolds number and consequently to the operating velocity, the first term increasing and the second decreasing as the Reynolds number increases. For optimization the conditions should be determined which minimize neither term by itself but which minimize the product of the two terms.

Equation 18 can also be written as:

$$i_{\text{opt}} = (B/A)^{1/2}(1 + C/B)^{1/2}. \tag{22}$$

This demonstrates that the optimum current density is greater than the optimum current density under hydrodynamically ideal conditions, $(B/A)^{1/2}$.

Inserting Equation 22 into 21 we obtain a form which is convenient for calculations:

$$\frac{(K - D)}{(K - D)_{\text{ideal}}} = \frac{1}{2}\left[\frac{i}{(B/A)^{1/2}} + \frac{(B/A)^{1/2}}{i}\left(1 + \frac{C}{B}\right)\right]. \tag{23}$$

The terms in Equation 23 can be identified as:

$$\frac{B}{A} = \frac{\bar{C}_s\eta_1}{C_e R_{\text{av}}} \tag{24}$$

$$1 + \frac{C}{B} = 1 + f(Re)^3 \cdot \frac{g + h}{g} \cdot \frac{C_e\mu^3}{\bar{C}_s D_e^3 \rho^2 \eta_2}. \tag{25}$$

In this analysis three useful dimensionless ratios have been developed. The normalized total sensitive cost:

$$(K - D)/(K - D)_{\text{ideal}}$$

is a ratio of those cost factors sensitive to current density to the same costs if the unit were run under hydrodynamically ideal conditions.

The group:

$$i\left(\frac{C_e R_{\text{av}}}{\bar{C}_s\eta_1}\right)^{1/2}$$

relates the operating current density to the optimum current density under hydrodynamically ideal conditions.

The third group, the energy cost ratio, subsequently designated N_{ec}:

$$\frac{C_e\mu^3}{C_s\rho^2 D_e^3\eta_2}$$

is a dimensionless ratio of energy cost to amortized area–proportional costs. In the dimensionless cost analysis these factors always occur as a ratio of one to the other.

5.1. *Hydrodynamic optimization*

The difficulty in hydrodynamic optimization is that there is a very large number of variables even after the simplification has been performed of expressing the relevant parameters dimensionlessly. Performance depends on promoter shape, pro-

moter size, promoter position in the channel, inter-promoter spacing and flow velocity. The several techniques used in this study are discussed below.

5.2. *Optimum promoter position*

For a particular promoter type, a general evaluation can be made of promoter position based on the observation that the pressure drop is determined for that type once the promoter spacing and the flow velocity is specified. It is possible on a plot of $D_e/\Delta l$ versus (Re) to indicate regions where the various positions (e.g. attached, opposed, alternating) of that promoter type give the highest overall mass transfer.

The boundaries of these regions are determined from the equations by equating the values of (Sh) in the two regions. For example, the boundary between attached and opposed is:

$$\frac{D_e}{\Delta l} = 2{\cdot}22(Re)^{-0{\cdot}567}. \qquad (26)$$

Having established the boundaries of the region we can determine the optimum promoter position in each region by comparing a calculated value in each region or by observing from the exponents in the equations given in Table 1 that opposed position will be best at high values of $D_e/\Delta l$ and that at low values of $D_e/\Delta l$ attached position will be best at low values of (Re). A plot of the preferred promoter position for rectangular promoters is given in Fig. 4. Note that while the boundaries are sharp, the difference in performance between adjacent positions is not very great near the boundaries.

A more general method is needed to permit comparison of rectangular and circular promoters, promoters with different contraction coefficients or spacers with different promoter spacings. Examination of Equation 23 and its expansion through Equations 24 and 25 shows that the normalized total cost depends on two dimensionless groups which are affected by system hydrodynamics, (Sh), which places an upper limit on the current density and the product $f(Re)^3$ which is proportional to the energy expenditure for pumping fluid through the unit. For convenience in plotting, the cube root of the latter factor is used. Both (Sh) and the pressure drop group $f^{1/3}(Re)$ increase with increasing linear velocity. The curve of (Sh) versus $f^{1/3}(Re)$ for a particular spacer

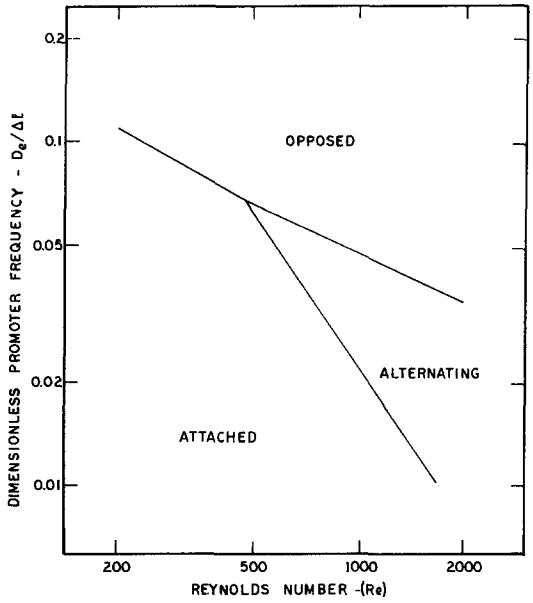

Fig. 4. Preferred promoter arrangement for rectangular promoters.

Table 1. Sherwood number correlations

Attached rectangular	$(Sh) = 1{\cdot}68(Sc)^{1/3}(Re)^{0{\cdot}343}(D_e/\Delta l)^{0{\cdot}284}$
Opposed rectangular	$(Sh) = 1{\cdot}38(Sc)^{1/3}(Re)^{0{\cdot}483}(D_e/\Delta l)^{0{\cdot}531}$
Alternating rectangular	$(Sh) = 1{\cdot}45(Sc)^{1/3}(Re)^{0{\cdot}378}(D_e/\Delta l)^{0{\cdot}309}$
Attached triangular	$(Sh) = 0{\cdot}318(Sc)^{1/3}(Re)^{0{\cdot}565}(D_e/\Delta l)^{0{\cdot}289}$
Opposed triangular	$(Sh) = 0{\cdot}196(Sc)^{1/3}(Re)^{0{\cdot}671}(D_e/\Delta l)^{0{\cdot}373}$
Detached triangular A	$(Sh) = 1{\cdot}47(Sc)^{1/3}(Re)^{0{\cdot}416}(D_e/\Delta l)^{0{\cdot}445}$
Detached triangular V	$(Sh) = 0{\cdot}045(Sc)^{1/3}(Re)^{0{\cdot}832}(D_e/\Delta l)^{0{\cdot}239}$
Attached circular $\beta = 0{\cdot}8$	$(Sh) = 0{\cdot}084(Sc)^{1/3}(Re)^{0{\cdot}696}(D_e/\Delta l)^{0{\cdot}269}$
Detached circular $\beta = 0{\cdot}8$	$(Sh) = 4{\cdot}24 \times 10^{-3}(Sc)^{1/3}(Re)^{1{\cdot}094}(D_e/\Delta l)^{0{\cdot}153}$
Detached circular $\beta = 0{\cdot}5$	$(Sh) = 0{\cdot}272(Sc)^{1/3}(Re)^{0{\cdot}631}(D_e/\Delta l)^{0{\cdot}357}$
Detached circular $\beta = 0{\cdot}34$	$(Sh) = 1{\cdot}33(Sc)^{1/3}(Re)^{0{\cdot}404}(D_e/\Delta l)^{0{\cdot}34}$

morphology is an almost straight line with a positive slope. The line which is higher and to the left indicates the better performance. If two lines cross, the point of intersection delimits the regions in which each is better. By plotting $(Sh)/(Sc)^{1/3}$ instead of (Sh), we obtain an evaluation which is independent of solution composition.

5.3. *Optimum promoter frequency*

For rectangular promoters Fig. 4 indicates that at high promoter frequencies, where the highest Sherwood numbers are to be found, the opposed position is preferred. The measured current densities diverged from the values calculated from the equation in Table 1 for the values of $D_e/\Delta l \geqq 0{\cdot}164$. In line with this, values of (Sh) for high promoter frequencies were adjusted downward.

Fig. 5 shows the effect of promoter frequency on spacer performance. The lines are drawn to cover the range of (Re) from 200 to 2000 where these values fit within the scope of the graph. In these calculations the values of (Sh) for $D_e/\Delta l = 0{\cdot}182$ were adjusted downward by 20%. This figure shows an optimum at approximately $D_e/\Delta l = 0{\cdot}12$. The optimum is fairly flat, the Sherwood numbers for the range of $D_e/\Delta l$ of 0·09 to 0·18 being within 11% of the best calculated value. The occurrence of the optimum at this relatively high value of $D_e/\Delta l$ bears out the presumption that the opposed position would be optimum for this promoter.

Similar plots showed that the optimum promoter freqeuncy is 0·12 for detached A position triangular promoters and that a promoter frequency of 0·18, the highest measured, was the best measured for detached circular promoters $\beta = 0{\cdot}5$.

Using the optimum or best measured value of promoter spacing for each promoter shape a general plot of promoter performance was assembled. This appears in Fig. 6. While there are a number of promoter types near the top of the chart, the detached circular promoters produced the best curves.

5.4. *Optimum contraction coefficient*

By observation of the three curves for detached circular promoters, the effect of promoter size relative to channel height can be seen. This comparison becomes a little more obvious if the curve for $\beta = 0{\cdot}8$ is hypothetically extended. It then can be seen that the optimum value of β increases as the Reynolds number increases.

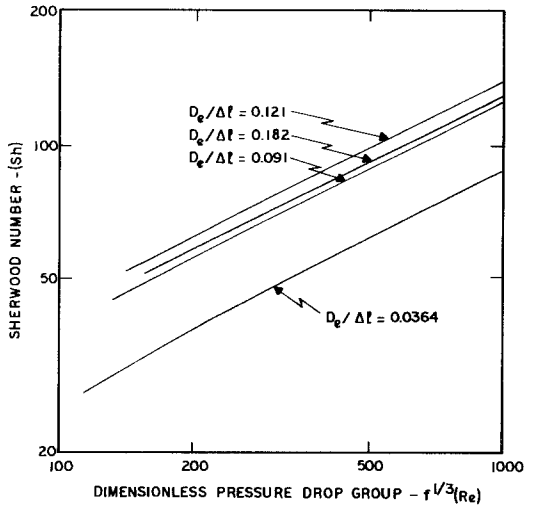

Fig. 5. Effect of promoter frequency on spacer performance for opposed rectangular promoters.

5.5. *Comparison with open channels*

One would normally employ turbulence promoters only if they produce a substantial improvement in performance. In laminar flow, f was calculated from Equation 4 and (Sh) from the dimensionless form of Equation 2 which is:

$$(Sh) = 1{\cdot}467(Sc)^{1/3}(Re)^{1/3}(D_e/h)^{1/3}(D_e/L)^{1/3}. \quad (27)$$

In turbulent flow the situation is made more difficult by the relative absence of good mass transfer correlations in the flow regime of interest. f was calculated from the Blasius equation [5]:

$$f = 0{\cdot}079(Re)^{-1/4}. \quad (28)$$

For mass transfer the Chilton–Colburn analogy was used, which according to Lin *et al.* [6] gives accurate values for short channels even for $(Re) =$ 2000 to 5000:

$$(Sh) = 0{\cdot}0395(Sc)^{1/3}(Re)^{3/4}. \quad (29)$$

For long channels the value of (Sh) at $(Re) = 2000$ may be one-half or less of the value predicted by Equation 29.

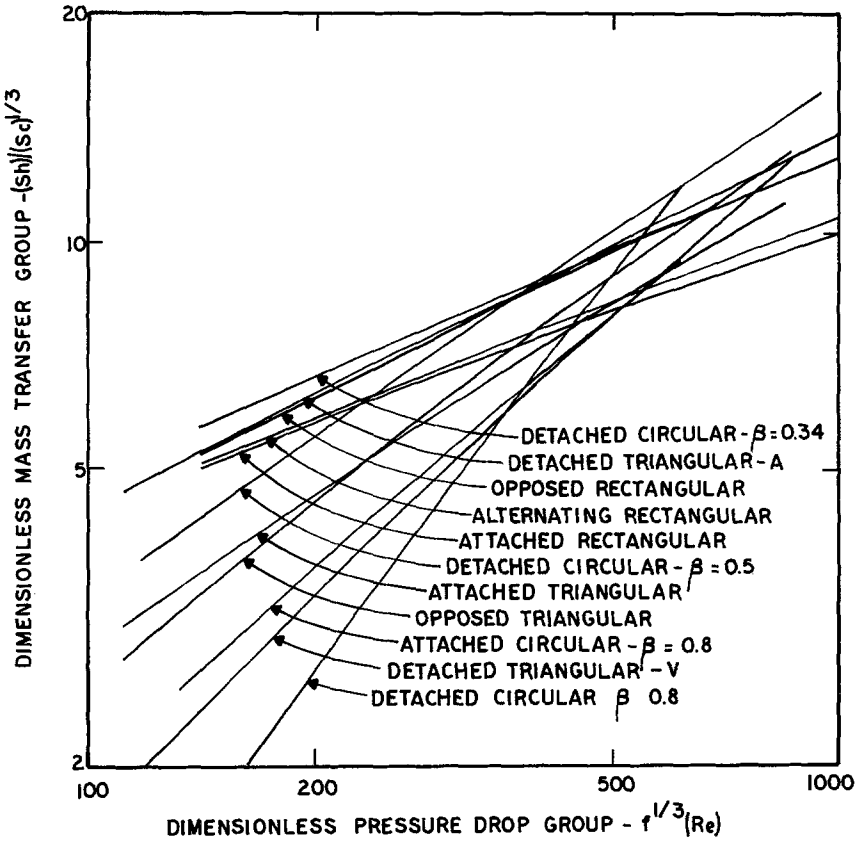

Fig. 6. General comparison of promoter types and arrangements at best promoter frequency for each type.

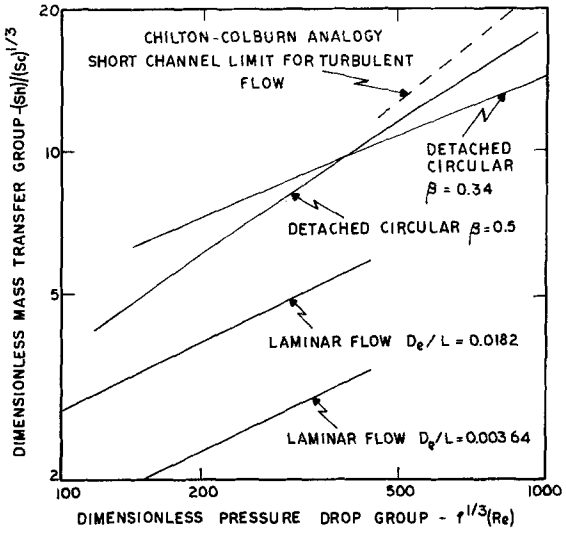

Fig. 7. Comparison of two best promoter morphologies with open channel in laminar flow and with short channel limit in turbulent flow.

In Fig. 7 the two best promoters are plotted on a field of $(Sh)/(Sc)^{1/3}$ versus $f^{1/3}(Re)$ compared to curves for a relatively long open channel in laminar flow, $D_e/L = 0{\cdot}00304$, and a relatively short open channel, $D_e/L = 0{\cdot}0182$. Compared to either of these, the use of turbulence promoters is a significant improvement. The Chilton–Colburn analogy is shown as a dotted line. For very short channels, use of turbulence promoters may not be an improvement over use of sufficient velocity to obtain turbulence. In this context, however, 'short' refers to a channel about as long as the spacing between promoters, for which we would not expect the promoter to be very useful. For longer channels the use of promoters will also be beneficial in the turbulent regime.

5.6. *Final optimization and evaluation*

The plot of $(Sh)/(Sc)^{1/3}$ versus $f^{1/3}(Re)$ does not

reveal the optimum flow condition or the economic benefit resulting from use of a particular spacer. This is obtained from a plot of $(K-D)/(K-D)_{opt}$ versus (Re).

In order to demonstrate the use of such a plot, calculations were made for a system with $N_{ec} = 1{\cdot}35 \times 10^{-10}$, $D_e/h = 1{\cdot}82$ and properties like those of a dilute solution of NaCl.

In order to demonstrate the effect of two kinds of promoters, Fig. 8 shows an open channel with $D_e/L = 0{\cdot}003\,64$, an alternating rectangular promoter, similar to the one in commercial use, with $D_e/\Delta l = 0{\cdot}182$ for which the Sherwood number was reduced by 20% as indicated above, and a detached circular promoter with $\beta = 0{\cdot}5$ and $D_e/\Delta l = 0{\cdot}182$. Because of the widely differing dependence of (Sh) and f on (Re), the curves have quite different shapes. Both promoters at optimum values of (Re) represent a considerable improvement over the open channel. As concluded from Fig. 6, the circular promoter is better than the rectangular promoter. From Fig. 8 it can be seen quantitatively how much better the circular promoter is. Further, the figure shows that the optimum Reynolds number for the circular promoter is higher than that for the rectangular promoter and the optimum for the circular promoter is broader allowing a wider range of operating flow velocities to be used.

Increasing the energy–area cost ratio moves the total cost away from the ideal cost and moves the optimum Reynolds number to higher values.

6. Conclusions

Local rates of mass transfer to a flat surface have been measured by an electrochemical process using a segmented electrode. This method is particularly useful in the hydrodynamic region near an obstruction.

This method has been used to obtain mass transfer profiles and average rates of mass transfer for several turbulence promoter shapes in various positions with respect to the polarizable surface. Comparison of mass transfer with promoters to performance in open channels demonstrates the significant improvements that can be made by the use of promoters.

A plot of $(Sh)/(Sc)^{1/3}$ versus $f^{1/3}(Re)$ yields a general relative evaluation of turbulence promoters. A plot of $(K-D)/(K-D)_{ideal}$ versus (Re) provides a means of determining the best operating conditions and of determining that portion of process cost which is attributable to hydrodynamic limitations.

Acknowledgement

The data in this paper were taken from a study supported by the Office of Saline Water, US Department of the Interior, Contract No. 14-01-001-2174. The encouragement and suggestions of Dr Sidney Johnson of that office are gratefully acknowledged.

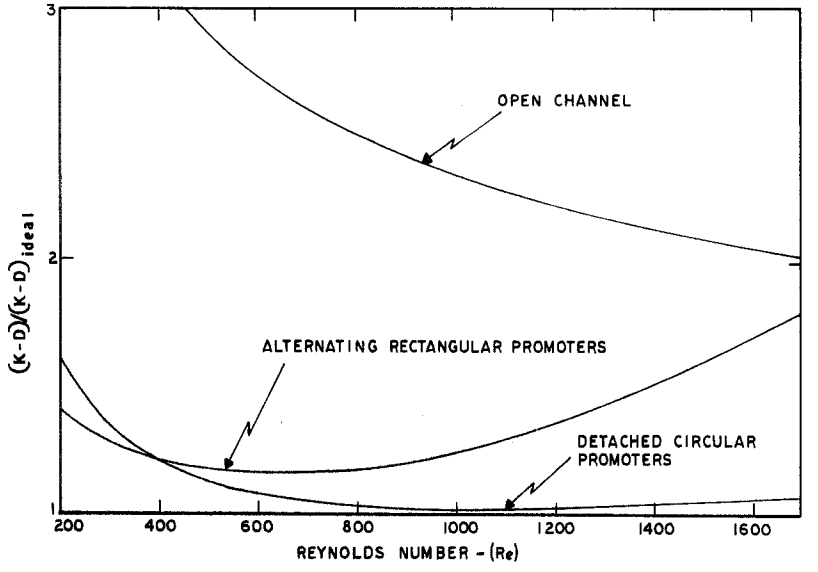

Fig. 8. Effect of promoters on system economics.

References

[1] P. H. Bradley, J. L. Greatorex and F. B. Leitz, 'Effect of Turbulence Promoters on Local Mass Transfer', Office of Saline Water R & D Report No. 597, Department of the Interior, December (1970).

[2] J. Newman, *Ind. Eng. Chem.* **60** (1968) 12.

[3] F. B. Leitz, L. Marinčić, P. Johnson and J. Liston, 'Effect of Turbulence Promoters on Local Mass Transfer – Second Report', Office of Saline Water, US Department of the Interior, June (1974).

[4] L. Marinčic and F. B. Leitz, 'Effect of Turbulence Promoters on Local Mass Transfer-Second Report', Office of Saline Water R&D Report No. 793, Department of the Interior, April (1973).

[5] H. Schlichting, 'Boundary Layer Theory', 4th edn, McGraw-Hill Book Company, New York (1960).

[6] C. S. Lin, E. B. Denton, H. S. Gaskill and G. L. Putnam, *Ind. Eng. Chem.* **43** (1951) 2136.